THE JOURNAL OF BIOLOGICAL CHEMISTRY VOL. 289, NO. 11, pp. 7994–8006, March 14, 2014
© 2014 by The American Society for Biochemistry and Molecular Biology, Inc. Published in the U.S.A.

Enhanced Enzyme Kinetic Stability by Increasing Rigidity within the Active Site*[S]

Received for publication, November 18, 2013, and in revised form, January 20, 2014 Published, JBC Papers in Press, January 21, 2014, DOI 10.1074/jbc.M113.536045

Yuan Xie[‡§], **Jiao An**[‡§], **Guangyu Yang**[‡], **Geng Wu**[‡], **Yong Zhang**[‡], **Li Cui**[‡], **and Yan Feng**[‡1]

From the [‡]*State Key Laboratory of Microbial Metabolism, School of Life Sciences and Biotechnology, Shanghai Jiao Tong University, Shanghai 200240, China and* [§]*Key Laboratory for Molecular Enzymology and Engineering of Ministry of Education, Jilin University, Changchun 130023, China*

Background: Improving the kinetic stability of enzymes is a key issue for protein engineers.
Results: Mutagenesis of residues with a high B factor located within 10 Å of the catalytic Ser^{105} residue enhances kinetic stability dramatically.
Conclusion: Increasing the rigidity of the flexible segment within the active site improves enzymatic kinetic stability.
Significance: Optimization of the active site may an alternative, efficient approach for enhancing protein stabilization.

Enzyme stability is an important issue for protein engineers. Understanding how rigidity in the active site affects protein kinetic stability will provide new insight into enzyme stabilization. In this study, we demonstrated enhanced kinetic stability of *Candida antarctica* lipase B (CalB) by mutating the structurally flexible residues within the active site. Six residues within 10 Å of the catalytic Ser^{105} residue with a high B factor were selected for iterative saturation mutagenesis. After screening 2200 colonies, we obtained the D223G/L278M mutant, which exhibited a 13-fold increase in half-life at 48 °C and a 12 °C higher T_{50}^{15}, the temperature at which enzyme activity is reduced to 50% after a 15-min heat treatment. Further characterization showed that global unfolding resistance against both thermal and chemical denaturation also improved. Analysis of the crystal structures of wild-type CalB and the D223G/L278M mutant revealed that the latter formed an extra main chain hydrogen bond network with seven structurally coupled residues within the flexible α10 helix that are primarily involved in forming the active site. Further investigation of the relative B factor profile and molecular dynamics simulation confirmed that the enhanced rigidity decreased fluctuation of the active site residues at high temperature. These results indicate that enhancing the rigidity of the flexible segment within the active site may provide an efficient method for improving enzyme kinetic stability.

Enzyme stability is a significant concern for protein engineers because of its great industrial importance. Numerous studies have revealed that enzymes maintain their structural stability through various kinds of non-covalent interactions, including hydrogen bonds, salt bridges, hydrophobic interactions, and van der Waals forces. Therefore, the most common strategy to improve enzymatic stability is to introduce new interactions that raise the transition state energy barrier for denaturation. In the past, stable biocatalysts were generated by amino acid substitution to increase structural rigidity (1–3), restrict conformational flexibility (4–11), and increase interactions between unstable domains (12–15). However, insufficient knowledge of the structure-function relationship hampered the identification of suitable targets for mutation. Exploring novel stabilization mechanisms and strategies for guiding enzyme design are therefore necessary.

Advances in structural biology and bioinformatics have provided new capabilities for evaluating the flexibility of segments/residues in a protein that have subsequently helped in the selection of key mutation sites for protein stabilization. Tian *et al.* (16) used molecular dynamics (MD)[2] simulation to select residues with high root mean square fluctuation (RMSF) values for mutation to proline to improve protein thermostability. Moreover, Joo *et al.* (17) achieved thermostabilization of *Bacillus circulans* xylanase by designing a flexible surface cavity using computational tools. The most technological advance thus far involves improving the thermostability of the smallest lipase in nature, namely *Bacillus subtilis* lipase (composed of 181 residues that form the core α/β-hydrolase fold), based on its B factor (18). This value represents the diffusion of atomic electron densities with respect to their equilibrium positions due to thermal motion and positional disorder. Thus, the B factor can be used to indicate the mobility of individual residues. Reetz *et al.* (18) chose 10 residues with a high B factor to construct iterative saturation mutagenesis libraries. After screening, the best mutant showed a half-life ($t_{1/2}$) at 55 °C of 980 min, which is

* This work was supported by the National Basic Research Program of China (973 Program Grants 2012CB721003 and 2011CBA00800), the Natural Science Foundation of China (Grant 31370106), and the National High Technology Research and Development Program of China (Grant 2013AA102801).

[S] This article contains supplemental Table S1.

The atomic coordinates and structure factors (codes 4K6G, 4K6H, 4K6K, and 4K5Q) have been deposited in the Protein Data Bank (http://wwpdb.org/).

[1] To whom correspondence should be addressed: State Key Laboratory of Microbial Metabolism, School of Life Sciences and Biotechnology, Shanghai Jiao Tong University, 800 Dongchuan Rd., Shanghai 200240, China. Tel.: 86-21-34207189; Fax: 86-21-34207189; E-mail: yfeng2009@sjtu.edu.cn.

[2] The abbreviations used are: MD, molecular dynamics; RMSF, root mean square fluctuation; CalB, *C. antarctica* lipase B; T_{50}^{15}, the temperature at which enzyme activity is reduced to 50% after a 15-min heat treatment; C_{50}, urea concentration at which an enzyme loses 50% activity upon incubation in urea for 24 h; *p*NP, *p*-nitrophenyl; RMSD, root mean square derivate; Bis-Tris, 2-[bis(2-hydroxyethyl)amino]-2-(hydroxymethyl)propane-1,3-diol.

Downloaded from http://www.jbc.org/ at BIRMINGHAM SOUTHERN COLLEGE on October 9, 2017

~490-fold higher than that of the wild-type protein. MD simulations have suggested that stepwise formation of an extensive hydrogen bond/salt bridge network of structurally coupled residues on the enzyme surface increases protein thermostability (19). Successful enhancement of *B. subtilis* lipase thermostability using this approach led to widespread focus on this strategy (20–22). However, the analysis of enzymes larger and more complex than *B. subtilis* lipase yielded inconclusive results. For example, when Kim *et al.* (21) mutated the seven residues with the highest B factor on the surface of *Candida antarctica* lipase B (CalB; composed of 317 residues that constitute a lid domain and extra secondary structures around the core α/β-hydrolase fold), they obtained a mutation that increased the $t_{1/2}$ at 50 °C (54 min) only 24%. This result implied that, because of the complexity of enzyme structures, only reducing the surface fluctuation may be insufficient for protecting the active site from heat-induced conformational changes that inactivate the enzyme.

Extensive research has resulted in two distinct definitions for *in vitro* protein stability, namely thermodynamic stability and kinetic stability. Thermodynamic stability involves the resistance of a folded protein conformation to denaturation, whereas kinetic stability measures its resistance to irreversible inactivation (23). Although enzyme unfolding and deactivation can sometimes be related, they are clearly the result of different processes. For most industrial enzymes, kinetic stability (*i.e.* loss of biological activity), not thermodynamic stability (*i.e.* protein unfolding), is the most important parameter used to describe overall stability (24). Comparative studies of the relationship between enzyme conformation and activity during denaturation suggest that the active site is more fragile than the enzyme as a whole (25, 26). Because the active site plays a key role in enzymatic catalysis, maintaining its correct conformation is the key to engineering its kinetic stability.

Therefore, we developed a novel method for enhancing the stability of CalB that involves mutating residues within its active site. This method increased the rigidity of the active site to protect the enzyme against irreversible inactivation under harsh conditions. Lipases catalyze a wide range of reactions, such as ester hydrolysis, esterification, and transesterification, thereby rending them important biocatalysts in the production of detergents, food, flavors, energy, and fine chemicals (27–31). Until now, scientists have used computational modeling (21), inserted extra disulfide bridges (22), and used error-prone PCR (32) to obtain more stable mutants. To understand how local active site rigidity impacts enzyme kinetic stability, we mutated residues that demonstrated high mobility within the active site. Residues with a high B factor and located within 10 Å of the catalytic Ser^{105} residue were chosen as candidates for constructing iterative saturation mutagenesis libraries. The kinetic stability and thermodynamic stability of the mutants were subjected to conditions that typically lead to heat- and chemical-induced denaturation. Furthermore, crystallography and MD simulation were performed to elucidate the structural basis for improved stability. Results from this study have substantiated the concept of local rigidity as an efficient strategy for improving enzyme kinetic stabilization. It should be noted that insights regarding local rigidity emphasize the significance of local rigidity in thermal stabilization.

EXPERIMENTAL PROCEDURES

Media and Reagents—The CalB gene was synthesized at GenScript Crop (Nanjing, China). Restriction enzyme and T4 ligase were purchased from New England Biolabs (Ipswich, MA). PrimeSTAR polymerase was purchased from TaKaRa (Dalian, China). The QIAquick™ PCR purification kit was purchased from Qiagen (Hilden, Germany). *Escherichia coli* Rosetta (DE3) competent cells and pET-22b were purchased from Novagen (Madison, WI). *E. coli* was routinely cultured overnight at 37 °C in 2× YT broth containing Bacto tryptone (1.6%, w/v), Bacto yeast extract (1%, w/v), and sodium chloride (0.5%, w/v) or on 2× YT agar plates with (in both cases) 100 μg/ml ampicillin. All substrates were purchased from Sigma.

In Silico Design Procedure—We used the crystal structure of *C. antarctica* lipase B (Protein Data Bank code 1TCA) to design thermostable CalB variants. For analyzing the flexibility of the protein, the B factor profile of Protein Data Bank code 1TCA was used. The amino acids located within 10 Å of the catalytic Ser^{105} residue, which showed a high B factor value, were chosen for saturation mutagenesis. Saturation mutagenesis libraries were created at amino acid positions Phe^{71}, Asp^{223}, Leu^{277}, Leu^{278}, Ala^{281}, and Ile^{285}.

In addition, regardless of the locations, the residues with the highest B factor values in CalB were also chosen as points for iterative saturation mutagenesis. Generally, the residues located on the protein surface have a higher B factor than residues in the protein core because few interactions are formed among surface residues. After deleting N-terminal and C-terminal amino acids, all sites were chosen on the surface of the protein (Arg^{249}, Arg^{309}, Arg^{242}, Glu^{269}, Leu^{219}, Lys^{13}, and Pro^{218}).

Recombinant Protein Expression and Purification—CalB gene (wild type) was amplified using primers containing the restriction sites for NcoI and XhoI (supplemental Table S1). Polymerase chain reaction (PCR) amplification was carried out with PrimeSTAR polymerase and a temperature program consisting of 98 °C for 2 min; 30 cycles of 10 s at 98 °C, 15 s at 55 °C, and 1 min at 72 °C; and a final 10-min extension at 72 °C. The PCR product was digested with NcoI and XhoI and subsequently cloned into the vector pET-22b (pET22b-WT). pET22b-WT was transformed into the Rosetta (DE3) by electroporation. The expression and purification of recombinant protein followed the described method (33).

Library Creation and Thermostability Screening—The mutants were prepared by whole-plasmid PCR with the primer containing NNK (sense strand)/MNN (antisense strand) degeneracy at those target sites (supplemental Table S1). Here N represents any of the following A, T, G, or C; K represents G or T; M represents A or C. PCR was performed with PrimeSTAR polymerase and a temperature program consisting of 98 °C for 2 min; 30 cycles of 10 s at 98 °C, 15 s at 55 °C, and 7 min at 72 °C; and a final 10-min extension at 72 °C. The PCR products were digested with DpnI to remove the parent plasmid and purified with a PCR purification kit. The created libraries were electroporated into Rosetta (DE3) cells and selected for ampicillin

Downloaded from http://www.jbc.org/ at BIRMINGHAM SOUTHERN COLLEGE on October 9, 2017

resistance. Cells were plated on 2× YT agar plates containing 100 μg/ml ampicillin and 0.5% (v/v) tributyrin emulsified in 0.4% (w/v) gum arabic followed by incubation at 37 °C for 8 h and then incubation at 15 °C for 24 h. The appearance of clear haloes around the colonies upon incubation indicates enzyme activity. All the clones that showed clear haloes were picked in 96-well plates containing 200 μl of 2× YT medium with 100 μg/ml ampicillin. After growth at 37 °C for 8 h, the cultures were used to inoculate fresh medium in an identical plate and incubated further for 3 h at 37 °C. After 1 mM isopropyl 1-thio-β-D-galactopyranoside was added, the cells were incubated for 24 h at 15 °C. Each saturation mutagenesis library contained 200 colonies.

Cells were harvested by spinning the plates at 4000 rpm for 30 min at 4 °C and lysed by a triple freeze-thaw from −80 °C, and then 200 μl of 50 mM sodium phosphate buffer (PBS, pH 7.5) was added in each well. The supernatant was divided into two identical 96-well PCR plates. One plate was incubated at high temperature for 15 min and cooled at 4 °C for 20 min followed by equilibration at room temperature for 15 min. The other plate was incubated under identical conditions except for incubation at high temperature. Screening of the thermostability of the mutants used *p*NP caprylate as the substrate, and hydrolysis was monitored at 405 nm for 2 min. The ratio of activity of each clone incubated at higher temperature *versus* control without incubation was taken as residual activity, which was used to identify the positive clones. A limited number of iterative saturation mutagenesis (18) experiments were performed in the next round by choosing the genes of some of the "best hits" as templates for randomizing at another amino acid position.

Enzyme Activity Assays—*p*NP caprylate was used to compare the activity of CalB variants. The ability of the enzyme to hydrolyze *p*NP caprylate was determined by measuring the absorbance of *p*-nitrophenol liberated using a UV-2550 spectrophotometer with a thermal control unit (Shimadzu, Kyoto, Japan). The reaction mixture consisted of 0.02 ml of 10 mM *p*NP caprylate as a substrate in acetonitrile and 0.97 ml of 50 mM PBS, pH 7.5 containing an appropriate amount (10 μl) of the enzyme solution. The enzyme reaction was performed for 1 min at 37 °C. The activities were determined photometrically at 37 °C, and the buffer was adjusted at 37 °C unless otherwise stated. One lipase unit in this assay is defined as the amount of enzyme that liberates 1 μmol of *p*-nitrophenol/min under these conditions.

The effect of temperature on the activity of lipase (1 μg/ml) was examined across the range 30–70 °C. The 50 mM PBS was adjusted to pH 7.5 at the respective temperature.

For the kinetic studies, the concentration of *p*NP caprylate increased from 50 to 1000 μM. The enzymatic activity of CalB variants was determined at different temperatures (293, 298, 303, 308, 313, 318, 323, and 328 K). Kinetic parameters V_{max} and K_m were acquired by fitting enzymatic activities as a function of substrate concentrations to the Michaelis-Menten equation using non-linear regression of the software Origin 8.0. The parameter k_{cat} was obtained by using the following equation: $k_{cat} = V_{max}/[E]$ where [E] is the molar concentration of the enzymes. Values of the free energy ($\Delta G^{\ddagger}$), enthalpy ($\Delta H^{\ddagger}$), and entropy ($\Delta S^{\ddagger}$) of activation at 308 K were calculated using the following equation: $\Delta G^{\ddagger} = RT(\ln k_B T/h - \ln k_{cat})$, $\Delta H^{\ddagger} = E_a - RT$, and $T\Delta S^{\ddagger} = \Delta G^{\ddagger} - \Delta H^{\ddagger}$ where k_B is the Boltzmann constant, h is the Planck constant, and R is the universal gas constant.

Thermal Inactivation and Unfolding—The CalB variants (0.1 mg/ml) were incubated at different temperatures for different time intervals from 0 to 150 min and then cooled on ice for 10 min. Their residual enzyme activities were assayed at 37 °C as described above. The data were fitted to first-order plots and analyzed with the first-order rate constants (k_d) determined by linear regression of ln(residual activity) *versus* the incubation time (t). The time required for the residual activity to be reduced to half ($t_{1/2}$) of the CalB variants was calculated using the following equation: $t_{1/2} = \ln 2/k_d$. The changes in transition state free energy ($\Delta\Delta G$) for inactivation between mutants and wild type were calculated using the following equation: $\Delta\Delta G = -RT \ln(k_{d\ mutant}/k_{d\ wild\ type})$ (34) where T and R are temperature and the gas constant (1.987 cal·K^{-1}·mol^{-1}), respectively. $\Delta\Delta G$ of wild type was used as a reference value. $k_{d\ wild\ type}$ and $k_{d\ mutant}$ were inactivation rate constants of wild-type and mutant CalB, respectively.

Heat treatment of purified protein was carried out by incubating the protein in 0.2-ml PCR tubes in a programmable thermal cycler for precise temperature control. Proteins (25 μl of 0.1 mg/ml in 50 mM PBS, pH 7.5) were heated at different temperatures for 15 min and cooled at 4 °C for 20 min followed by equilibration at room temperature for 15 min. Samples were centrifuged to remove any aggregated protein before assaying for enzymatic activity. The activity at 37 °C was considered to be 100%; the residual activities were quantitatively measured after heating at different temperatures for 15 min. The T_{50}^{15} value is the temperature at which enzyme activity is reduced to 50% after a 15-min heat treatment. The precise value was obtained by determination of the inflection point of a fit of the residual activities at certain temperatures to a sigmoidal plot (sigmoidal Boltzmann fit using Origin 8.0) (35).

Differential Scanning Calorimetry—All differential scanning calorimetry measurements were performed on a VP-Capillary differential scanning calorimeter (MicroCal, LLC) from GE Healthcare. Samples were degassed by stirring gently under vacuum prior to measurements. Protein samples were diluted to 2.5 mg/ml by 12.5 mM PBS, pH 7.5, and the corresponding buffer was used as a reference. Protein unfolding events were recorded between 25 and 85 °C with a scan rate of 2.0 K/min with an initial 21 min of equilibration at 25 °C. The scans were analyzed after subtraction of an instrument baseline recorded with buffer in both cells using the software package Origin provided by the manufacturer.

Urea-induced Unfolding—The enzyme inactivation was induced by incubating ~0.03 mg/ml proteins with a set of concentrations of urea for 24 h at room temperature. The residual activities of the enzymes were measured at 37 °C using *p*NP caprylate as the substrate in 50 mM PBS, pH 7.5 containing the corresponding concentration of urea. The C_{50} value, indicating the concentration of urea in which 50% of enzymatic activity was retained, was calculated as T_{50}^{15}.

Downloaded from http://www.jbc.org/ at BIRMINGHAM SOUTHERN COLLEGE on October 9, 2017

For fluorescence measurements, samples treated similarly were measured on an F-7000 fluorescence spectrophotometer (Hitachi, Japan) at 20 °C. Samples were excited at 282 nm to monitor the tryptophan emission with a slit width of 5 nm for both excitation and emission. Spectra were recorded from 300 to 400 nm at a scanning speed of 1200 nm/min. The scanning experiments were performed three times, and the processed data were given as the means of three measurements. The shift in wavelength maximum was used to monitor the conformational change at various denaturant concentrations. All the sample spectra were corrected for background fluorescence. The data for wild type and mutants were analyzed by a two-state model using Origin 8.0 according to the equation: $S_{obs} = (S_N + S_U e^{(-(\Delta G - md)/RT)})/(1 + e^{(-(\Delta G - md)/RT)})$ where S_{obs} is the observed spectroscopic signal, S_N and S_U are the signals for the native and unfolded species, respectively, ΔG is the free energy of unfolding in the absence of denaturant, m is the partial derivative of ΔG with respect to denaturant, and d is the concentration of denaturant. S_{obs} and d are the dependent and independent variables; S_N, S_U, ΔG, and m are treated as fitting parameters (36). The C_m, the urea concentration at the midpoint of urea-induced unfolding curve, was obtained using the following equation: $C_m = \Delta G/m$.

Crystallization of CalB Wild Type and Mutants—Crystals of CalB and its mutants were grown at 14 °C by the hanging drop, vapor diffusion method. All crystals were grown in 25% PEG 3350, 0.2 M sodium acetate, 0.1 M Bis-Tris, pH 6.5 and cryoprotected by the addition of 20% ethylene glycol (v/v) to the crystallization conditions. 1.5–1.6-Å-resolution data sets were collected at the beamline BL17U1 at Shanghai Synchrotron Radiation Facility (China). All data sets were integrated, scaled, and reduced with the HKL2000 software package. The structures were solved by molecular replacement with the CCP4i program PHASER using the structure of *C. antarctica* lipase B (Protein Data Bank code 1TCA) as the model. Model building was performed by COOT, and all of the model qualities were checked with PROCHECK. All molecular structures were visualized by PyMOL software. Hydrophobic interactions, disulfide bridges, hydrogen bonds, ionic interactions, aromatic-aromatic interactions, aromatic-sulfur interactions, and cation-pi interactions in the whole protein were calculated using the Protein Interactions Calculator (37), and all parameters were given default values.

MD Simulation—The crystal structures of wild type (Protein Data Bank code 4K6G) and mutants (L278M, Protein Data Bank code 4K6H; D223G/L278M, Protein Data Bank code 4K5Q) were further optimized by energy minimization using the conjugate gradient algorithm supplement in Discovery Studio 3.0 (Accelrys, San Diego, CA). CHARMM force field and Momany-Rone partial charge were used to assign atom types. Maximum steps and root mean square gradient values were set to 10,000 and 0.001, respectively. An implicit solvent model was used, and the dielectric constants of protein and solvent were set to 1 and 80, respectively. Other parameters were set to default values.

The MD simulation was performed using GROMACS v4.5.5 (38) implementing the GROMACS 96.1 (53a6) force field. The initial structure was solvated with a simple point-charge model of water in a box. A sufficient number of Na^+ ions were added to neutralize the negative charges in the system. The system was then subjected to a steepest descent energy minimization and the 30-ps MD simulation was performed at 300 K with the heavy atoms and Cα atoms fixed. Finally, a 30-ns MD simulation was performed on the whole system at 300 and 330 K. All bond lengths were constrained using the Linear Constraint Solver (LINCS) algorithm. The cutoff value for van der Waals interactions was set at 1 nm, and electrostatic interactions were calculated using a particle mesh Ewald algorithm. The time step of the simulations was set at 2 fs, and the coordinates were saved for analysis every 2 ps. Postprocessing and analysis were performed using standard GROMACS tools and Visual Molecular Dynamics (VMD).

RESULTS

Construction of Iterative Saturation Mutagenesis Libraries—CalB is a globular α/β-hydrolase that is $\sim 30 \times 40 \times 50$ Å in size with a catalytic triad composed of Ser^{105}, Asp^{187}, and His^{224}. Its substrate binding pocket is an elliptical, steep funnel 9.5×4.5 Å in size. The catalytic Ser^{105} residue is located within the tight turn between β4 and helix α4 at the bottom of the binding pocket. When bound, the substrate is oriented parallel to the long axis of the active site (39). To identify residues that play a role in enhancing the local stability of the CalB active site, we mutated amino acids based on two criteria: 1) location within a 10-Å radius around the Ser^{105} residue and 2) a relatively high B factor. As shown in Fig. 1, six residues with an average B factor over 10 were selected using B-FITTER (40) based on the published x-ray crystallography structure of CalB (Protein Data Bank code 1TCA). These resides were Leu^{278}, Ile^{285}, Leu^{277}, Ala^{281} (all located within the α10 helix), Phe^{71} (located in the loop connecting the β3 strand and α3 helix), and Asp^{223} (located in the loop connecting the α8 and α9 helices) (Fig. 1). Saturation mutagenesis libraries of these residues were generated and screened for enhanced thermostability. To ensure reasonable coverage of the relevant protein sequence, 200 transformants were screened for each library (41). We found that amino acids 278, 281, and 285 were crucial for enzymatic activity because mutation led to a dramatic alteration in activity (data not shown). Heat treatment (55 °C for 15 min) identified several positive mutants in the Leu^{278} and Asp^{223} libraries. In particular, sequencing revealed that the most thermostable mutants were L278M and D223G.

To further improve enzyme stability, the gene encoding L278M was used as a template for iterative saturation mutagenesis at the other five sites (Ile^{285}, Leu^{277}, Ala^{281}, Phe^{71}, and Asp^{223}). Mutagenesis of Phe^{71} and Asp^{223} did not significantly impact enzymatic activity; however, mutagenesis of Leu^{277}, Ala^{281}, and Ile^{285} resulted in large fluctuations in enzyme activity. Heating these five libraries at 59 °C for 15 min revealed that the best variant was L278M/D223G from the L278M/D223*X* library. Additional iterative saturation mutagenesis of the remaining four residues using L278M/D223G as a template did not further improve thermostability. More importantly, the enzyme lost most of its activity following multiple mutations within the active site.

Downloaded from http://www.jbc.org/ at BIRMINGHAM SOUTHERN COLLEGE on October 9, 2017

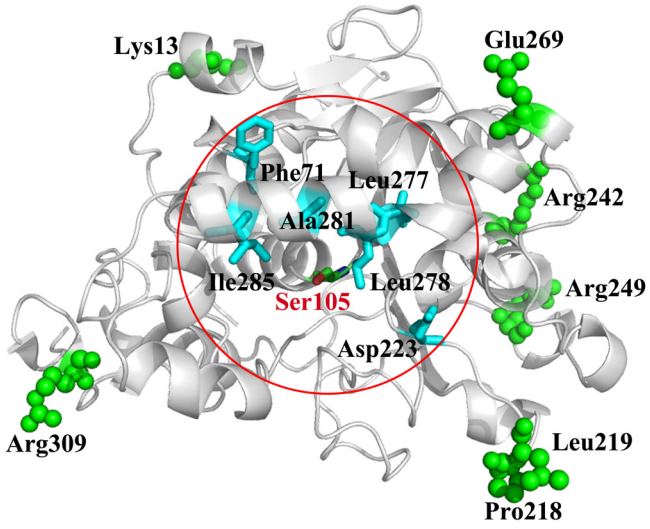

	Selected residues on the surface							Selected residues within 10 Å around Ser105					
Residues	Arg^{249}	Arg^{309}	Arg^{242}	Glu^{269}	Leu^{219}	Lys^{13}	Pro^{218}	Leu^{278}	Ile^{285}	Leu^{277}	Ala^{281}	Phe^{71}	Asp^{223}
B factor	27.5	26.31	25.22	24.52	23.65	20.6	20.4	15.99	13.34	11.98	11.17	11.13	10.14
Distance (Å)	28.6	28.1	26.7	26.0	25.2	26.5	21.5	7.5	8.3	9.5	8.4	9.7	10.0

FIGURE 1. **CalB sites chosen for iterative saturation mutagenesis.** The diagram shows a structural model based on the x-ray crystallographic structure of CalB (Protein Data Bank code 1TCA). Mutation sites around the catalytic Ser^{105} residue are shown in *cyan*: Leu^{278}, Ile^{285}, Leu^{277}, Ala^{281}, Phe^{71}, and Asp^{223}. Mutation sites on the protein surface are shown in *green*: Arg^{249}, Arg^{309}, Arg^{242}, Glu^{269}, Pro^{218}, Leu^{219}, and Lys^{13}. The B factor and distances between the side chains of selected residues and Ser^{105} residue were measured. The Ser^{105} residue is shown in *stick* form, and the area within 10 Å of this residue is outlined with a *red circle*.

TABLE 1

Kinetic stability properties of wild-type and mutant CalB

Values represent the mean of three independent sets of experiments with S.D. <5%. —, not detected.

CalB variants	k_d [a]	$t_{1/2}$ [b]	$\Delta\Delta G$ [c]	T_{50}^{15} [d]	C_{50} [e]
	min^{-1}	*min*	$kJ \cdot mol^{-1}$	°C	M
Wild type	0.1816 ± 0.01	3.8 ± 0.2	—	46.4 ± 0.3	2.07 ± 0.07
D223G	0.052 ± 0.002	13.4 ± 0.6	3.1 ± 0.1	48.8 ± 0.3	2.75 ± 0.10
L278M	0.0287 ± 0.0003	24.2 ± 0.3	4.6 ± 0.1	50.2 ± 0.1	2.87 ± 0.06
D223G/L278M	0.0141 ± 0.0007	49.2 ± 2.5	6.3 ± 0.1	58.5 ± 0.3	2.90 ± 0.10
A281E		—[f]			

[a] k_d denotes the first-order rate constants of inactivation at 48 °C.
[b] $t_{1/2}$ represents the half-life at 48 °C and is equal to ln $2/k_d$.
[c] $\Delta\Delta G = -RT \ln(k_{d\ mutant}/k_{d\ wild\ type})$.
[d] Temperature at which enzymes lose 50% activity after incubation for 15 min.
[e] Urea concentration at which enzymes lose 50% activity after treatment for 24 h.
[f] This mutant was deactivated too rapidly to measure at 48 °C. The half-life was less than 5 min at only 45 °C.

For comparison, residues located on the surface of CalB were also investigated using a similar method. Seven residues with high B factors were chosen for saturation mutagenesis, namely Arg^{249}, Arg^{309}, Arg^{242}, Glu^{269}, Leu^{219}, Lys^{13}, and Pro^{218} (Fig. 1). The average B factors of these residues were much higher than those of residues within the active site. With the exception of those from the Pro^{218} library, most of the mutants retained their catalytic activity (data not shown). No obvious thermostable variants were found in all the libraries examined under the same screening conditions.

Kinetic, Dynamic, and Chemical Stability of the CalB Variants—Irreversible thermal inactivation is an important parameter for describing the kinetic stability of enzymes. To assess this property, each variant was incubated at 48 °C and then cooled on ice for 10 min before the residual activity was measured at 37 °C with respect to the time of incubation. All traces of thermal inactivation were found to follow first-order kinetics. Calculation of the $t_{1/2}$ and transition state free energy ($\Delta\Delta G$) of the CalB variants was based on the inactivation constant k_d. As shown in Table 1, the $t_{1/2}$ of D223G/L278M at 48 °C was 49 min, which was about 13-fold higher than that of wild type. Thermodynamic analysis showed that the $\Delta\Delta G$ of D223G/L278M, L278M, and D223G increased by 6.3, 4.6, and 3.1 $kJ \cdot mol^{-1}$, respectively, compared with wild type. The higher $\Delta\Delta G$ exhibited by D223G/L278M suggests that it possesses higher energy barriers against thermal inactivation, thus making it more stable than other single variants.

The temperature at which 50% of enzyme activity remains after incubation for 15 min (T_{50}^{15}) is another parameter used to evaluate kinetic stability. The activity of the CalB variants was assessed by incubating each enzyme from 37 to 65 °C. No significant differences in residual activity were observed with treatment below 40 °C (Fig. 2*A*). However, incubation at temperatures above 45 °C affected this activity. For example, at 50 °C, the residual activity of wild-type CalB was only 14% after treatment; however, D223G and L278M retained ~45% activ-

Downloaded from http://www.jbc.org/ at BIRMINGHAM SOUTHERN COLLEGE on October 9, 2017

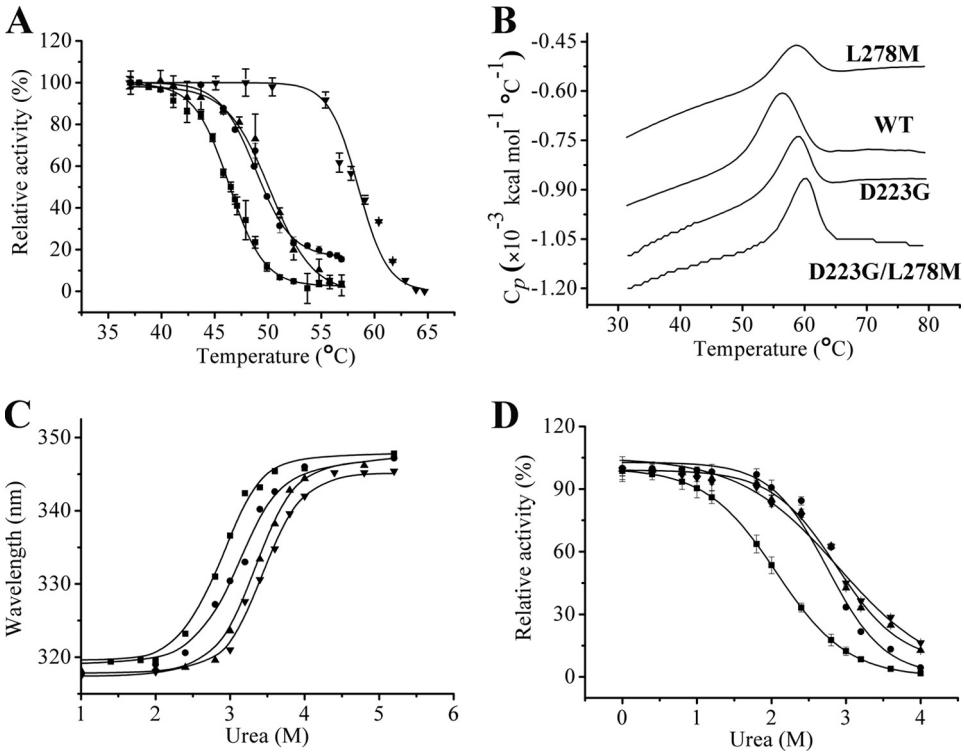

FIGURE 2. **Thermally and urea-induced inactivation/unfolding profiles of wild-type and mutant CalB.** *A*, thermal inactivation profiles of CalB mutants. Enzymes in 50 mM sodium phosphate buffer, pH 7.5 were incubated at various temperatures for 15 min and assayed for residual activity at 37 °C. The activity measured at 37 °C was considered to be 100%. *B*, results from differential scanning calorimetric analysis of the CalB mutants. The scans were analyzed after subtraction of an instrument-derived baseline recorded with buffer in both cells as calculated using the Origin software package. *C*, the fluorescence spectra were recorded at wavelengths between 300 and 400 nm with an excitation wavelength at 282 nm under a scanning speed of 1200 nm/min. *D*, urea-induced inactivation profiles of wild-type and mutant CalB. Enzymes were incubated with different concentrations of urea for 24 h and then assayed for residual activity at 37 °C. Activity measured in the absence of urea was considered to be 100%. ■, wild type; ●, D223G; ▲, L278M; ▼, D223G/L278M. The fitted curves for protein unfolding are shown as *black lines*. *Error bars* represent S.D.

TABLE 2

Thermodynamic properties of wild-type and mutant CalB

Values represent the mean of three independent sets of experiments with S.D. <5%.

Mutant	T_m	ΔH_u	ΔS_u	C_m[a]
	°C	kJ·mol^{-1}	J·mol^{-1}·K^{-1}	M
Wild type	56.0 ± 0.05	114.5 ± 0.7	348.0 ± 2.3	2.9 ± 0.05
D223G	58.4 ± 0.1	104.4 ± 1.7	314.9 ± 5.2	3.1 ± 0.03
L278M	58.3 ± 0.2	87.7 ± 1.6	264.6 ± 4.7	3.3 ± 0.2
D223G/L278M	59.6 ± 0.1	129.2 ± 1.6	388.4 ± 4.7	3.4 ± 0.1

[a] Midpoint of transition as determined by a red shift in fluorescence emission maxima.

ity, whereas D223G/L278M retained ~86% activity. The $T_{50}{}^{15}$ of D223G and L278M was higher by 2.4 and 3.8 °C, respectively, compared with wild type (Table 1). Unexpectedly, $T_{50}{}^{15}$ of the best variant, D223G/L278M, increased to 58.5 °C, which is ~12 °C higher than that of wild type. This result demonstrated that a strong synergistic effect exists between D223G and L278M to enhance CalB kinetic stability, thereby leading D223G/L278M to greater kinetic stability than wild type.

To investigate the thermodynamic effect of the mutants, the melting temperature (T_m) of each CalB variant was measured by differential scanning calorimetry. Because a single peak appeared in the scans, we inferred that the wild type and three CalB variants underwent a single transition (Fig. 2*B*). As shown in Table 2, the T_m values for D223G, L278M, and D223G/L278M were 2.4, 2.3, and 3.6 °C higher than that of wild type (56 °C), respectively. Unlike the change in kinetic stability ($T_{50}{}^{15}$), no synergistic effect between D223G and L278M was observed on the thermodynamic stability (T_m) of CalB.

To further examine changes in thermodynamic stability, the enthalpy (ΔH_u) and entropy (ΔS_u) of the unfolding process were calculated by non-linear fitting (Table 2). Although ΔH_u and ΔS_u of the single mutants decreased, both values increased in the double mutants. This result indicates that improving the stability of the double mutant was not due to a simple additive effect of the two single mutations.

In D223G/L278M, when the temperature was equal to T_m, ΔH_u and $T\Delta S_u$ canceled each other out. However, when the temperature was lower than T_m, ΔH_u became larger than $T\Delta S_u$, resulting in a more positive ΔG_u value that reflects enhanced stability. Therefore, mutants exhibiting a higher ΔH_u value may be more stable when $T < T_m$. This conclusion is consistent with the fact that a high ΔH_u value for D223G/L278M indicates that it has greater stability (*e.g.* longer $t_{1/2}$ and higher $T_{50}{}^{15}$) than other variants when $T < T_m$. Moreover, enhancement of ΔH_u contributed to increased thermodynamic stability of the double mutant.

To assess the chemical stability of the variants, urea-induced protein unfolding was performed. The maximum emission wavelength shift in intrinsic fluorescence was used as a measure of the global conformational change (Fig. 2*C*). The urea concentration at the unfolding curve midpoint (C_m) of wild-type CalB was 2.89 M. This value shifted 0.25, 0.43, and 0.55 M higher in concentration for D223G, L278M, and D223G/L278M,

Downloaded from http://www.jbc.org/ at BIRMINGHAM SOUTHERN COLLEGE on October 9, 2017

respectively (Table 2). The mutants also exhibited better chemical resistance than wild type in the urea-induced inactivation assay (Fig. 2*D* and Table 1). After treatment with 2.4 M urea for 24 h, wild-type CalB retained only 33% of its original activity, whereas all the mutants retained ~62% activity. The C_{50} value, which indicates the urea concentration that inhibits 50% of the enzymatic activity, increased 0.7, 0.8, and 0.8 M for D223G, L278M, and D223G/L278M, respectively. These results indicate that mutations within the active site could improve the thermal and chemical stability of CalB.

Catalytic Properties of CalB Variants—The specific activity of wild-type CalB and D223G, L278M, and D223G/L278M mutants was determined at temperatures ranging from 25 to 70 °C using *p*NP caprylate as the substrate. The optimal temperature for catalytic activity by the mutants increased to 57.5, 57.5, and 62.5 °C for D223G, L278M, and D223G/L278M, respectively, which is 2.5–7.5 °C higher than that of wild-type CalB (Fig. 3). Results from further analysis of the enzymatic activity of CalB variants at different temperatures are represented in the Arrhenius plot ($\ln k_{cat}$ *versus* $1/T$) shown in Fig. 3 (*inset*). The activation energy (E_a) of the reactions was calculated from the slope of the Arrhenius plot (Table 3). D223G displayed an E_a similar to that of wild type, whereas the E_a value of L278M was greater. In contrast, the E_a of D223G/L278M (43.24 kJ·mol^{-1}) was lower than that of wild type (45.23 kJ·mol^{-1}), suggesting that the double mutation results in a weaker temperature dependence for enzymatic activity and a broader temperature range for catalytic activity (Fig. 3).

Using *p*NP caprylate as the substrate, we determined the kinetic parameters of wild-type CalB and its mutants. All mutants except D223G, which demonstrated a minor decrease in k_{cat}, showed an increase in both k_{cat} and K_m compared with wild type (Table 3). L278M displayed the highest catalytic efficiency (k_{cat}/K_m) because its k_{cat} value was nearly 2.0-fold higher than that of wild type. The other two mutants, however, showed catalytic efficiency similar to that of wild type. Taken together, these results showed that the mutants possessed enhanced kinetic stability without sacrificing catalytic activity.

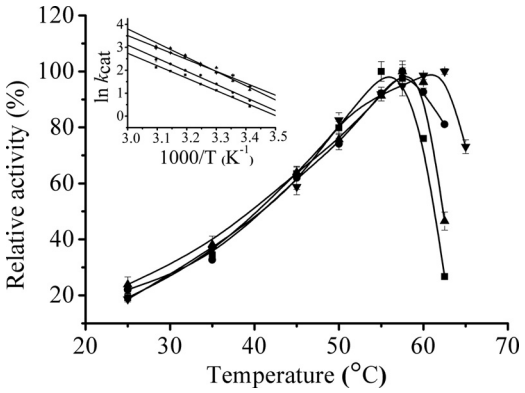

FIGURE 3. **Temperature dependence of wild-type and mutant CalB.** Enzymes were incubated at various temperatures for 1 min prior to activity measurement at the same temperature after the addition of substrate. The temperature-k_{cat} profile according to the Arrhenius plot is also shown (*inset*). ■, wild type; ●, D223G; ▲, L278M; ▼, D223G/L278M. *Error bars* represent S.D.

To provide additional insight into how the mutations affected CalB enzymatic activity, we calculated the free energy ($\Delta G^{\ddagger}$), enthalpy ($\Delta H^{\ddagger}$), and entropy ($\Delta S^{\ddagger}$) of activation (Table 3). $\Delta G^{\ddagger}$ is the difference in free energy between the transition state intermediate and the reactant. The $\Delta G^{\ddagger}$ value of each mutant was lower than that of wild type at 35 °C, suggesting that the rate of formation of mutant intermediates was faster than that of wild type.

Crystal Structure Analysis and MD Simulation—To gain insight into how the conformation produced by the various mutations increased CalB stability, we performed x-ray crystallography on each mutant. The data for wild-type and mutant CalB (except D223G segment 141–146, which was missing) are summarized in Table 4. The resolution was 1.5, 1.6, 1.6, and 1.5 Å for wild-type CalB and D223G, L278M, and D223G/L278M mutants, respectively. Superimposing the mutant structure onto the wild-type structure revealed that the root mean square deviation (RMSD) of the Cα position of D223G, L278M, and D223G/L278M was similar (0.266, 0.063, and 0.121, respectively) (Fig. 4*A*). The D233G mutation was located in front of the catalytic His^{224} residue, whereas the L278M mutation resided in the middle of the long C-terminal α10 helix, which lines the channel leading into the active site (42). Compared with wild type, no obvious increase in interaction was observed in the mutant structures (Table 5). Even the most stable mutant, D223G/L278M, exhibited fewer hydrogen bonds and ionic interactions despite the additional aromatic-sulfur interaction. Therefore, our data indicate that enhanced stability in the mutants was not the result of a greater number of interactions. Instead, we found that the critical difference between the mutants and wild-type CalB involved the types of interactions introduced into the active site. The L278M mutation resulted in a slight shift of the main chain of surrounding residues that induced a new aromatic-sulfur interaction between Met^{278} and Trp^{104} while simultaneously eliminating the aromatic-sulfur interaction between Met^{298} and Tyr^{300} and introducing two new hydrogen bonds (Fig. 4, *B* and *C*, and Table 6). In D223G/L278M, the mutations caused tighter compaction of the α10 helix. Compared with wild-type CalB (Fig. 4*B*), the position of the main chain oxygen atom of Pro^{268}, Lys^{271}, Ala^{274}, Ala^{275}, and Ala^{279} moved ~0.2–0.4 Å, and the position of the main

TABLE 3

Kinetic constants of wild-type and mutant CalB

Values represent the mean of three independent sets of experiments with S.D. <5%.

Mutant	K_m[a]	k_{cat}	k_{cat}/K_m	E_a	$\Delta G^{\ddagger}$	$\Delta H^{\ddagger}$	$\Delta S^{\ddagger}$
	μM	min^{-1}	$min^{-1}\mu M^{-1}$	kJ·mol^{-1}	kJ·mol^{-1}	kJ·mol^{-1}	J·mol^{-1}·K^{-1}
Wild type	9.5 ± 0.2	365 ± 10.5	38.4 ± 0.9	45.2 ± 0.3	70.9 ± 0.01	43.0 ± 0.3	−91.7 ± 0.09
D223G	10.7 ± 0.6	357 ± 39.5	33.4 ± 1.5	45.4 ± 0.02	68.6 ± 0.01	43.0 ± 0.02	−83.7 ± 0.09
L278M	11.1 ± 0.3	597 ± 8.5	54.0 ± 1.2	51.4 ± 0.2	67.4 ± 0.04	49.0 ± 0.2	−60.0 ± 0.90
D223G/L278M	14.6 ± 0.9	559 ± 7.2	38.4 ± 1.9	43.2 ± 0.2	67.5 ± 0.04	40.0 ± 0.2	−87.0 ± 0.80

[a] The kinetic constants were determined at 35 °C using *p*-NP caprylate as the substrate.

Downloaded from http://www.jbc.org/ at BIRMINGHAM SOUTHERN COLLEGE on October 9, 2017

TABLE 4
Data collection and refinement statistics

	Structure			
	WT CalB	**D223G**	**L278M**	**D223G/L278M**
Data collection statistics				
Cell parameter	a = 47.70 Å, b = 81.64 Å, c = 71.65 Å, $\alpha = \gamma = 90°$, β = 95.87°	a = 46.71 Å, b = 87.09 Å, c = 138.87 Å, $\alpha = \beta = \gamma = 90°$	a = 47.71 Å, b = 81.28 Å, c = 71.56 Å, $\alpha = \gamma = 90°$, β = 95.86°	a = 45.77 Å, b = 145.97 Å, c = 86.40 Å, $\alpha = \beta = \gamma = 90°$
Space group	$P2_1$	$P2_12_12_1$	$P2_1$	$C222_1$
Wavelength used (Å)	0.97916	0.97916	0.97916	0.97916
Resolution (Å)	50.0–1.5 (1.55–1.5)[a]	50.0–1.6 (1.66–1.60)	50.0–1.6 (1.66–1.60)	50.0–1.5 (1.55–1.5)
No. of molecules/asymmetric unit	2	2	2	1
No. of unique reflections	171,636	71,410	70,860	46,677
No. of all reflections	650,362	449,700	424,145	683,995
Completeness (%)	99.9 (100)	94.2 (95.8)	99.3 (100)	91.3 (100)
Redundancy	3.8 (3.7)	6.3 (6.2)	6.0 (6.1)	14.4 (14.5)
$I/\sigma(I)$	12.2 (6.3)	10.5 (4.0)	17.0 (5.8)	29.5 (13.7)
R_{merge}[b] (%)	9.7 (18.9)	11.8 (45.3)	8.4 (34.6)	7.3 (21.5)
Refinement statistics				
R_{work}[c] (%)	18.99	23.49	19.69	20.16
R_{free}[c] (%)	20.31	26.56	21.99	21.64
RMSD bond lengths (Å)	0.005	0.008	0.006	0.005
RMSD bond angle (°)	1.1	1.2	1.1	1.1
Overall B factor (Å^2)	11.42	13.79	15.46	17.43
Final model no. of protein atoms	4,645	4,572	4,677	2,318
Final model H_2O molecules	403	246	319	268
Ramachandran plot				
Residues in most favored regions	605	592	612	304
Residues in additionally allowed regions	21	21	21	10
Residues in generously allowed regions	2	2	2	1
Protein Data Bank code	4K6G	4K6K	4K6H	4K5Q

[a] Values in parentheses correspond to the highest resolution shell.
[b] $R_{merge} = \Sigma_{hkl}\Sigma_i|I(hkl)_i - I(hkl)|/\Sigma_{hkl}\Sigma_i(hkl)_i$ where $I(hkl)$ is the mean intensity of the observations $I(hkl)_i$ of reflection hkl.
[c] $R_{work} = \Sigma||F_{obs}| - |F_{calc}||/\Sigma|F_{obs}|$ where F_{obs} and F_{calc} are the observed and calculated structure factor amplitudes, respectively. R_{free} was calculated as R_{work} using a randomly selected subset consisting of ~10% of unique reflections not used for structure refinement.

chain nitrogen atom of Ala^{276}, Leu^{277}, and Ala^{279} shifted ~0.2–0.5 Å. Together with the change in the dihedral angle, these subtle structural adjustments induced a new hydrogen bond network involving six pairs of hydrogen bonds on segment 268–281 that strengthens its rigidity (Fig. 4*D* and Table 6). Meanwhile, an extra aromatic-sulfur interaction between Met^{278} and Trp^{104} allowed simultaneous maintenance of the other six aromatic-sulfur interactions (Fig. 4*E* and Table 5).

Calculation of the B factor from x-ray crystallographic data is frequently used to determine the distribution of flexible regions within a protein. Because crystallization conditions and resolution affect the B factor, we used a relative B factor value to indicate the relative rigidity of peptide segments within the entire protein. The residue with the highest B factor was set as 100%, and the relative B factors for the other residues were calculated accordingly. In D223G/L278M, we found significantly lower relative B factors in regions 211–226 and 257–281 (Fig. 5), indicating enhanced rigidity in these two segments. The enhanced rigidity at 257–281 correlated well with the formation of a new hydrogen bond network with the 268–281 segment. On the contrary, only a subtle change in relative B factor was observed in L278M (data not shown).

Next, we conducted MD simulation at 300 and 330 K to further assess the improved stability of the CalB mutants. The RMSD values of the backbone atoms of the CalB variants are shown in Fig. 6 for which the reference structure was obtained from the equilibration step performed immediately before the MD simulation run. The RMSD values of wild-type CalB demonstrated much greater fluctuation between 300 and 330 K than the mutants, which is consistent with the fact that the mutants possessed greater thermostability.

RMSF values often reflect the fluctuation of individual residues during the MD simulation process. As shown in Fig. 7, wild-type CalB possesses two major unstable regions, namely a segment of the α5 helix (142–148) and the initial portion of the α10 helix (267–286). The α5 helix resides on the lid domain, whose intrinsically high flexibility is beneficial for binding substrate and promoting catalysis. This helix exhibited high flexibility in wild-type CalB and the D223G/L278M mutant. Nevertheless, the behavior of the α10 helix was different between the two enzymes. In wild-type CalB, fluctuation of this region was higher at 330 K than at 300 K, suggesting that it is a highly flexible region during heat treatment. However, the D223G/L278M mutant showed considerably greater structural rigidity compared with wild type at both 300 and 330 K (Fig. 7), which is consistent with their relative B factor profiles (Fig. 5). These data reflect a novel approach for enhancing the stability of CalB that involves increasing the local rigidity of its active site.

DISCUSSION

Low stability often limits the usefulness of an enzyme industrially. In this study, we conducted iterative saturation mutagenesis on the structurally flexible residues of the active

Downloaded from http://www.jbc.org/ at BIRMINGHAM SOUTHERN COLLEGE on October 9, 2017

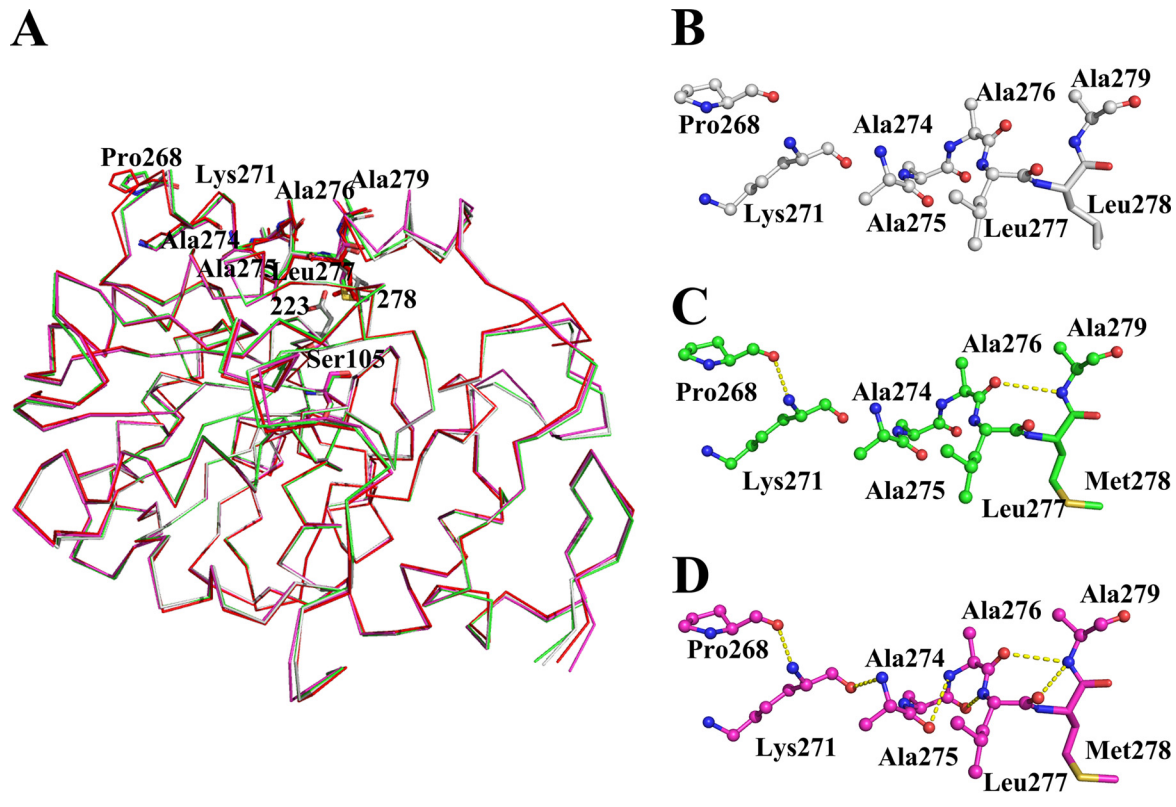

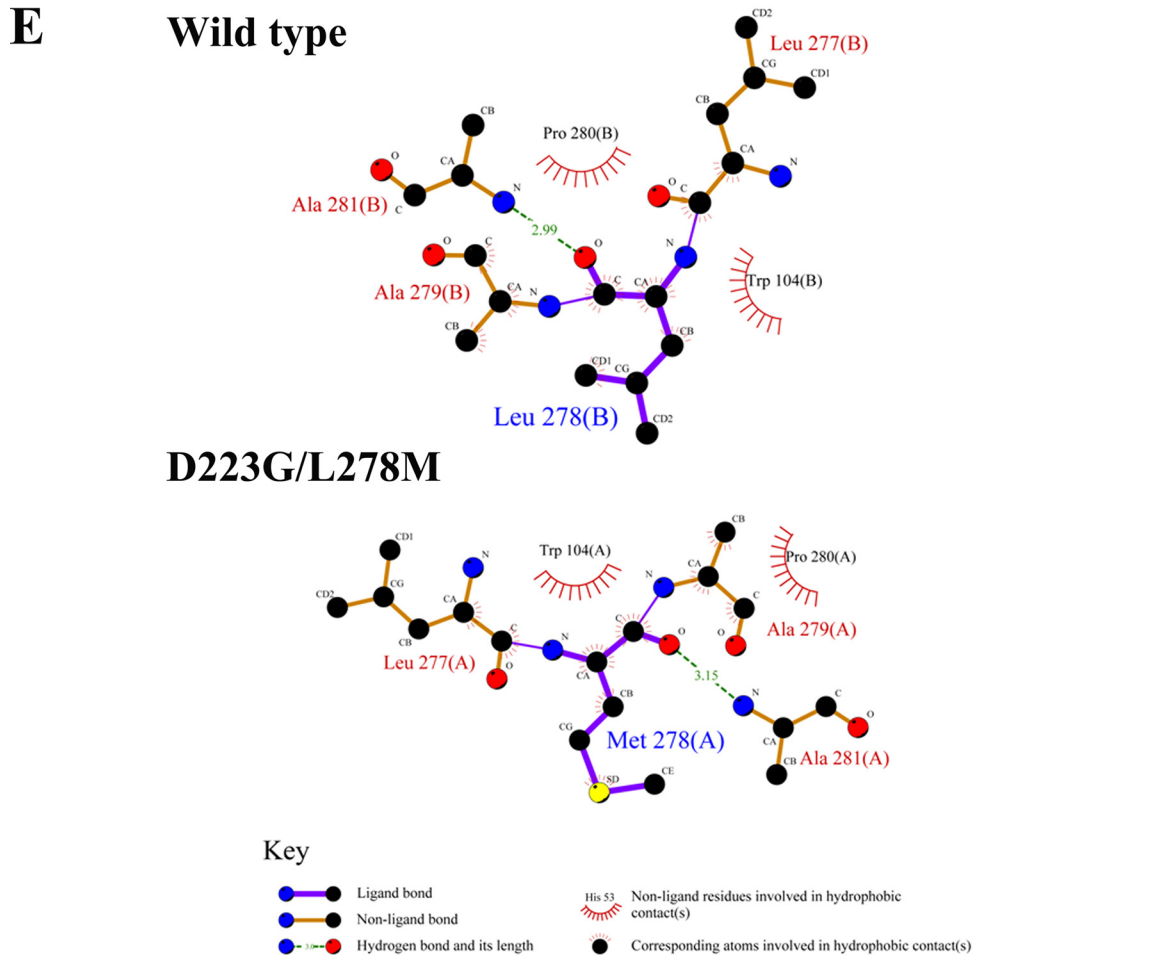

Downloaded from http://www.jbc.org/ at BIRMINGHAM SOUTHERN COLLEGE on October 9, 2017

site of *C. antarctica* lipase B to identify a very robust variant, D223G/L278M. Its kinetic stability was enhanced significantly as evidenced by a 13-fold increase in half-life at 48 °C and a 12 °C rise in T_{50}[15]. Additionally, the dynamic and chemical stability of the mutant improved without sacrificing activity. To our knowledge, this is the first report demonstrating that increasing the rigidity of its active site can enhance the kinetic stability of an enzyme.

In our previous work, we found that local interaction at the N-terminal region or on the interdomain interface could significantly affect the stability of a hyperthermophilic acylpeptide hydrolase from the archaeon *Aeropyrum pernix* K1 (4, 12). Koudelakova *et al.* (43) recently reported that the stability and resistance to organic cosolvent of haloalkane dehalogenase DhaA from *Rhodococcus rhodochrous* NCIMB 13064 could be adjusted by modifying the rigidity of the access tunnel. Because the kinetic stability of an enzyme is dependent on a subtle balance between the flexibility and rigidity of its active site, we reasoned that optimizing the rigidity of the active site may be an efficient method for enhancing kinetic stability of an enzyme. This modification may protect the enzyme against irreversible inactivation under harsh conditions. Moreover, it allows for

TABLE 5

Interactions potentially involved in the stability of wild-type and mutant CalB

Interactions	Wild type	L278M	D223G/L278M
Hydrophobic interactions	266	265	265
Disulfide bridges	3	3	3
Main chain-main chain hydrogen bonds	375	371	371
Main chain-side chain hydrogen bonds	192	189	189
Side chain-side chain hydrogen bonds	121	120	112
Ionic interactions	8	8	6
Aromatic-aromatic interactions	10	10	10
Aromatic-sulphur interactions	6	6	7
Cation-π interactions	4	3	3

TABLE 6

Extra main chain-main chain hydrogen bond interactions and shift of crucial atoms in CalB mutants compared with wild type

Distances and dihedral angles were measured using PyMOL.

L278M			D223G/L278M		
Extra MC-MC hydrogen bonds[a]	Distance change of correlated atoms[b]	Dihedrals angle change of correlated bonds[c]	Extra MC-MC hydrogen bonds	Distance change of correlated atoms	Dihedral angle change of correlated bonds
Å	Å	°	Å	Å	°
$P268O_{atom}$/$271N_{atom}$ (Dd-a = 3.44)	$P268O_{atom}$, 0.2	$P268O_{atom}$–Cα bond, 2.6	$P268O_{atom}$/$K271N_{atom}$ (Dd-a = 3.3)	$P268O_{atom}$, 0.3	$P268O_{atom}$–Cα bond, 8.3
	$K271N_{atom}$, 0.2	$K271N_{atom}$–Cα bond, 0.2		$K271N_{atom}$, 0.1	$K271N_{atom}$–Cα bond, 1.5
$A276O_{atom}$/$A279N_{atom}$ (Dd-a = 3.5)	$A276O_{atom}$, 0.1	$A276O_{atom}$–Cα bond, 1.2	$K271O_{atom}$/$A274N_{atom}$ (Dd-a = 3.4)	$K271O_{atom}$, 0.3	$K271O_{atom}$–Cα bond, 1.9
	$A279N_{atom}$, 0.4	$A279N_{atom}$–Cα bond, 1.1		$A274N_{atom}$, 0.1	$A274N_{atom}$–Cα bond, 1.4
			$A274O_{atom}$/$A276N_{atom}$ (Dd-a = 3.3)	$A274O_{atom}$, 0.2	$A274O_{atom}$–Cα bond, 3.2
				$A276N_{atom}$, 0.2	$A276N_{atom}$–Cα bond, 0.9
			$A276O_{atom}$/$A279N_{atom}$ (Dd-a = 3.4)	$A276O_{atom}$, 0.2	$A276O_{atom}$–Cα bond, 5.8
				$A279N_{atom}$, 0.5	$A279N_{atom}$–Cα bond, 2.2
			$L277O_{atom}$/$A279N_{atom}$ (Dd-a = 3.2)	$L277O_{atom}$, 0.1	$A277O_{atom}$–Cα bond, 1.7
			$A275O_{atom}$/$L277N_{atom}$ (Dd-a = 3.4)	$L277N_{atom}$, 0.2	$L277N_{atom}$–Cα bond, 1.4
				$A275O_{atom}$, 0.4	$A275O_{atom}$–Cα bond, 3.3

[a] Extra main chain-main chain hydrogen bond interactions induced by mutations. MC, main chain; N_{atom}, main chain nitrogen atom; O_{atom}, main chain oxygen atom; Dd-a, the distance between the proton donor and acceptor.
[b] Change in distance of the correlated atoms between wild-type and mutant CalB.
[c] Change in dihedral angle of correlated bonds between wild-type and mutant CalB.

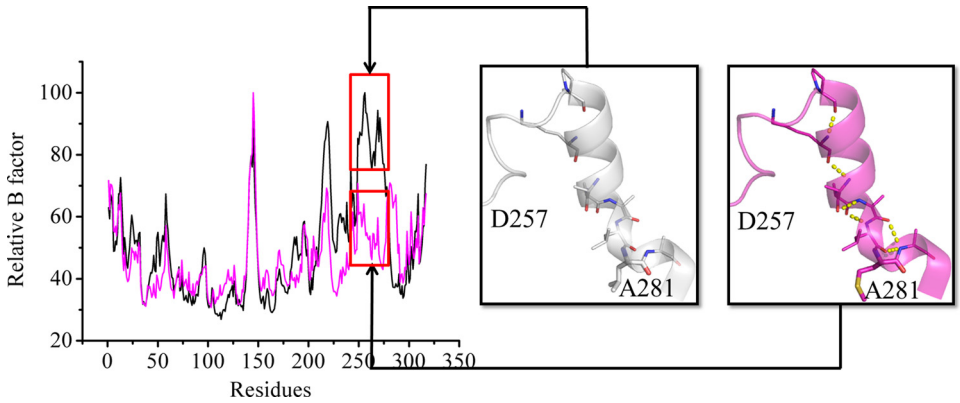

FIGURE 5. **Relative B factor profiles for wild-type (*black*) and D223G/L278M (*magenta*) CalB.** With the highest residue B factor set at 100%, the relative residue B factors for the entire protein were calculated. Structures of the 257–281 segment for wild-type CalB and D223G/L278M mutant are shown. The crucial amino acids are shown with *lines*, and the extra network of hydrogen bonds is shown as *yellow dashed lines*.

FIGURE 4. **Three-dimensional structure superimposition and hydrogen bond analysis in the CalB mutants.** *A*, structure alignment of wild-type (*white*) and mutant CalB. The D223G, L278M, and D223G/L278M mutants are depicted in *red*, *green*, and *magenta*, respectively. Crucial amino acids are shown as *lines*, whereas Ser^{105} residue and the D223G and L278M mutants are shown in *stick* form. *B*, crucial amino acids in wild-type CalB. *C*, crucial amino acids in L278M. *D*, crucial amino acids in D223G/L278M. *E*, interactions between amino acid 278 and other residues in wild-type CalB and the D223G/L278M mutant. Crucial amino acids are shown in *ball* and *line*, whereas L278/M278 is shown in *stick* form. *Yellow dashed lines* indicate the extended network of hydrogen bonds.

Downloaded from http://www.jbc.org/ at BIRMINGHAM SOUTHERN COLLEGE on October 9, 2017

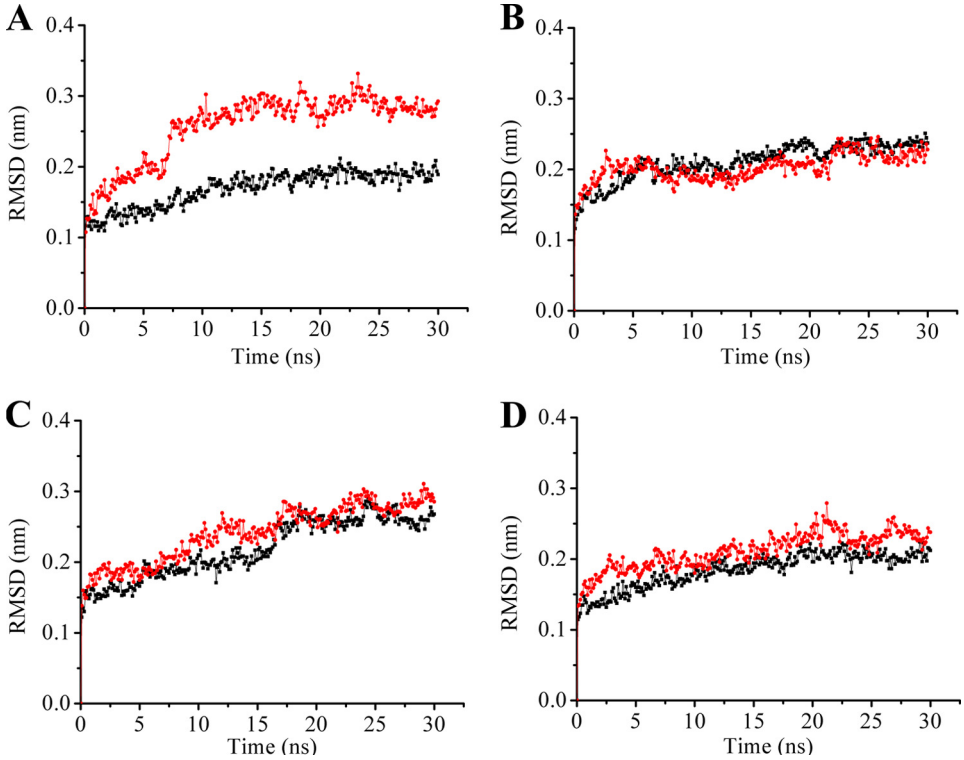

FIGURE 6. **RMSD values during a 30-ns MD simulation for wild-type and mutant CalB.** RMSD profiles of wild-type (*A*), D233G (*B*), L278M (*C*), and D233G/L278M (*D*) CalB at 300 and 330 K. RMSD values at 300 and 330 K are shown in *black* and *red*, respectively.

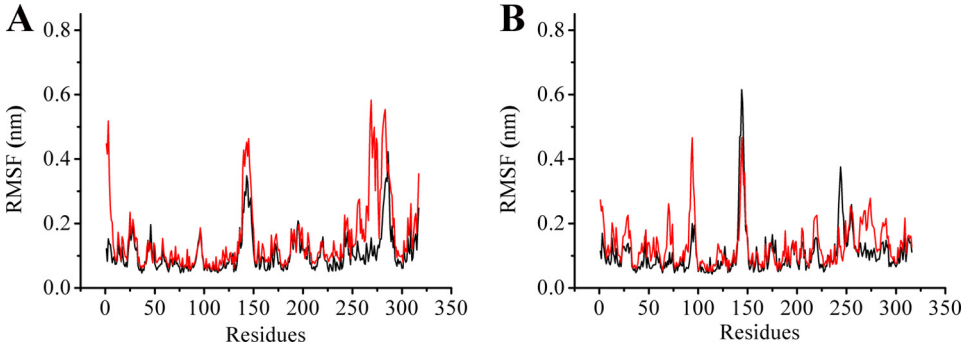

FIGURE 7. **RMSF values during a 30-ns molecular dynamic simulation for wild-type and D223G/L278M CalB at 300 and 330 K.** *A*, RMSF profile of wild-type CalB at 300 and 330 K. *B*, RMSF profile of D223G/L278M at 300 and 330 K. RMSF values at 300 and 330 K are shown in *black* and *red*, respectively.

the generation of mutants that perform better at elevated temperatures.

Indeed, data from this study showed that CalB mutants with significantly enhanced stability could be created using this new strategy. The best mutant, D223G/L278M, showed a greater improvement in stability than most previously published work (21, 22). It should be noted that Zhang *et al.* (32) screened a random mutagenesis library to identify a CalB mutant (A281E) that exhibited as much as 20-fold greater thermostability at 70 °C. However, we did not find any stabilization effect at position Ala^{281} by site-directed mutagenesis or screening of the site saturation mutagenesis library (Table 1). Our results suggest that focusing the mutagenesis effort on the active site creates "smarter" libraries that are more likely to yield positive results. Moreover, this approach is more feasible than other methods that require an in-depth knowledge of the structural features of the enzyme.

Data from high resolution crystal structures of wild-type and mutant CalB also provided important insights into the source of stability in the mutants. No obvious changes in interaction were observed in the L278M and D223G single mutants. However, when both mutations were present, their synergistic actions introduced an extra hydrogen bond network on segment 269–281 that increased the rigidity of the segments (Fig. 4*D* and Table 6).

Long MD simulations of CalB in aqueous solvent confirmed high mobility in the regions lining the channel that lead into the active site, especially the α5 and α10 helices (42). We postulated that the segment between 268 and 287, which exhibited great flexibility, is susceptible to disruption at elevated denaturing conditions. This movement exposes the active site to the external environment, thereby inactivating the enzyme. Enhanced rigidity in this segment could help the enzyme maintain its correct conformation at high temperature, prevent exposure of the active site, and improve its kinetic stability.

Downloaded from http://www.jbc.org/ at BIRMINGHAM SOUTHERN COLLEGE on October 9, 2017

This hypothesis was corroborated by relative B factor profiles and RMSF analysis (Figs. 5 and 7). The segment exhibited greater flexibility than other parts of the protein but displayed a notable decrease in flexibility (due to increased rigidity) in the presence of both mutations. This result demonstrates that even minimal structural modification can create sufficient conformational change to enhance thermostability. Our data also demonstrate the formation of an extra hydrogen bond network between atoms on the main chain of the protein rather than the side chains. For many years, enhanced enzymatic stability was achieved by introducing new side chain interactions because the main chain residues exhibited little change following mutagenesis (14, 19, 44). However, our results indicate that the accumulation of subtle hydrogen bond interactions between the main chain residues also contributes to enzyme stabilization. It should also be noted that the flexible secondary structure could be made even more rigid by further tightening the main chain interactions.

Enhancing stability while retaining enzymatic activity is a demanding task for protein engineering, particularly when improvements to stability are achieved through mutagenesis of residues within the active site. Because of high flexibility and the conservation of structure and sequences, any mutation within the active site can inactivate the enzyme. In this study, we successfully utilized a two-step screening method to increase the stability of CalB without sacrificing its activity. It is notable that the catalytic efficiency (k_{cat}/K_m) of all the mutants was not compromised in lieu of enhanced stability at all temperatures. Indeed, the relative B factor and RMSF profiles indicated that, with the exception of the flexible α10 helix (257–281), the backbone dynamic of the mutant did not change relative to the wild type (Figs. 5 and 7). This simultaneous improvement in stability and activity, which is reportedly uncommon, provides insight into how such mutations should be designed. While screening the iterative saturation mutagenesis libraries, we discovered that A281F and I285F exhibited even more specific activity than the wild type. The specific activity was 100.3 and 100 units/mg for A281F and I285F, respectively, compared with that of wild-type CalB, which was 20 units/mg. Both sites are located within the substrate-binding tunnel and are involved in enzyme-substrate binding. The introduction of more hydrophobic, larger side chains at these positions may facilitate substrate binding and/or catalysis, thereby leading to improved enzymatic activity. This result highlights the fact that mutagenesis of the structurally flexible residues within the active site can enhance kinetic stability and increase enzymatic activity.

CONCLUSIONS

In this study, we demonstrate the enhancement of *C. antarctica* lipase B kinetic stability by increasing the rigidity of its active site. Although some reports revealed that mutagenesis of high B factor sites/regions may enhance enzyme stability, our specific focus on the flexible residues within the active site allowed us to understand how local rigidity affects enzyme kinetic stability. The increased intermolecular interactions, particularly the main chain hydrogen bond network, contribute to higher kinetic stability and thus the maintenance of enzymatic activity at elevated temperatures. MD simulation in combination with analysis of the relative B factors suggests that a balance between flexibility (α5 helix) and rigidity (α10 helix) in the active site is essential for catalysis. Additional structural and biochemical assays will be performed on other enzymes to reveal the generality of this local stabilization strategy. Nevertheless, our results will help elucidate the properties that confer thermostability in enzymes and thus provide insight into how to design more efficient and thermostable biocatalysts.

REFERENCES

1. Yi, Z. L., Pei, X. Q., and Wu, Z. L. (2011) Introduction of glycine and proline residues onto protein surface increases the thermostability of endoglucanase CelA from *Clostridium thermocellum*. *Bioresour. Technol.* **102,** 3636–3638
2. Masui, A., Fujiwara, N., and Imanaka, T. (1994) Stabilization and rational design of serine protease AprM under highly alkaline and high-temperature conditions. *Appl. Environ. Microbiol.* **60,** 3579–3584
3. Liang, X., Bian, Y., Tang, X. F., Xiao, G., and Tang, B. (2010) Enhancement of keratinolytic activity of a thermophilic subtilase by improving its autolysis resistance and thermostability under reducing conditions. *Appl. Microbiol. Biotechnol.* **87,** 999–1006
4. Yang, G., Bai, A., Gao, L., Zhang, Z., Zheng, B., and Feng, Y. (2009) Glu88 in the non-catalytic domain of acylpeptide hydrolase plays dual roles: charge neutralization for enzymatic activity and formation of salt bridge for thermodynamic stability. *Biochim. Biophys. Acta* **1794,** 94–102
5. Voutilainen, S. P., Boer, H., Alapuranen, M., Jänis, J., Vehmaanperä, J., and Koivula, A. (2009) Improving the thermostability and activity of *Melanocarpus albomyces* cellobiohydrolase Cel7B. *Appl. Microbiol. Biotechnol.* **83,** 261–272
6. Imani, M., Hosseinkhani, S., Ahmadian, S., and Nazari, M. (2010) Design and introduction of a disulfide bridge in firefly luciferase: increase of thermostability and decrease of pH sensitivity. *Photochem. Photobiol. Sci.* **9,** 1167–1177
7. Yu, X. W., Tan, N. J., Xiao, R., and Xu, Y. (2012) Engineering a disulfide bond in the lid hinge region of *Rhizopus chinensis* lipase: increased thermostability and altered acyl chain length specificity. *PLoS One* **7,** e46388
8. Voutilainen, S. P., Murray, P. G., Tuohy, M. G., and Koivula, A. (2010) Expression of *Talaromyces emersonii* cellobiohydrolase Cel7A in *Saccharomyces cerevisiae* and rational mutagenesis to improve its thermostability and activity. *Protein Eng. Des. Sel.* **23,** 69–79
9. Yun, B. Y., Jun, S. Y., Kim, N. A., Yoon, B. Y., Piao, S., Park, S. H., Jeong, S. H., Lee, H., and Ha, N. C. (2011) Crystal structure and thermostability of a putative α-glucosidase from *Thermotoga neapolitana*. *Biochem. Biophys. Res. Commun.* **416,** 92–98
10. Perl, D., and Schmid, F. X. (2002) Some like it hot: the molecular determinants of protein thermostability. *ChemBioChem* **3,** 39–44
11. Gallardo, O., Pastor, F. I., Polaina, J., Diaz, P., Łysek, R., Vogel, P., Isorna, P., , B., and Sanz-Aparicio, J. (2010) Structural insights into the specificity of Xyn10B from *Paenibacillus barcinonensis* and its improved stability by forced protein evolution. *J. Biol. Chem.* **285,** 2721–2733
12. Zhang, Z., Zheng, B., Wang, Y., Chen, Y., Manco, G., and Feng, Y. (2008) The conserved N-terminal helix of acylpeptide hydrolase from archaeon *Aeropyrum pernix* K1 is important for its hyperthermophilic activity. *Biochim. Biophys. Acta* **1784,** 1176–1183
13. Kamondi, S., Szilágyi, A., Barna, L., and Závodszky, P. (2008) Engineering the thermostability of a TIM-barrel enzyme by rational family shuffling. *Biochem. Biophys. Res. Commun.* **374,** 725–730
14. Acharya, P., Rajakumara, E., Sankaranarayanan, R., and Rao, N. M. (2004) Structural basis of selection and thermostability of laboratory evolved *Bacillus subtilis* lipase. *J. Mol. Biol.* **341,** 1271–1281
15. Kamal, M. Z., Ahmad, S., Molugu, T. R., Vijayalakshmi, A., Deshmukh, M. V., Sankaranarayanan, R., and Rao, N. M. (2011) *In vitro* evolved non-aggregating and thermostable lipase: structural and thermodynamic investigation. *J. Mol. Biol.* **413,** 726–741

Downloaded from http://www.jbc.org/ at BIRMINGHAM SOUTHERN COLLEGE on October 9, 2017

16. Tian, J., Wang, P., Gao, S., Chu, X., Wu, N., and Fan, Y. (2010) Enhanced thermostability of methyl parathion hydrolase from *Ochrobactrum* sp. M231 by rational engineering of a glycine to proline mutation. *FEBS J.* **277,** 4901–4908
17. Joo, J. C., Pohkrel, S., Pack, S. P., and Yoo, Y. J. (2010) Thermostabilization of *Bacillus circulans* xylanase via computational design of a flexible surface cavity. *J. Biotechnol.* **146,** 31–39
18. Reetz, M. T., Carballeira, J. D., and Vogel, A. (2006) Iterative saturation mutagenesis on the basis of B factors as a strategy for increasing protein thermostability. *Angew. Chem. Int. Ed. Engl.* **45,** 7745–7751
19. Reetz, M. T., Soni, P., Acevedo, J. P., and Sanchis, J. (2009) Creation of an amino acid network of structurally coupled residues in the directed evolution of a thermostable enzyme. *Angew. Chem. Int. Ed. Engl.* **48,** 8268–8272
20. Zhang, J. H., Lin, Y., Sun, Y. F., Ye, Y. R., Zheng, S. P., and Han, S. Y. (2012) High-throughput screening of B factor saturation mutated *Rhizomucor miehei* lipase thermostability based on synthetic reaction. *Enzyme Microb. Technol.* **50,** 325–330
21. Kim, H. S., Le, Q. A. T., and Kim, Y. H. (2010) Development of thermostable lipase B from *Candida antarctica* (CalB) through *in silico* design employing B-factor and RosettaDesign. *Enzyme Microb. Technol.* **47,** 1–5
22. Le, Q. A., Joo, J. C., Yoo, Y. J., and Kim, Y. H. (2012) Development of thermostable *Candida antarctica* lipase B through novel *in-silico* design of disulfide bridge. *Biotechnol. Bioeng.* **109,** 867–876
23. Iyer, P. V., and Ananthanarayan, L. (2008) Enzyme stability and stabilization—aqueous and non-aqueous environment. *Process Biochem.* **43,** 1019–1032
24. Eijsink, V. G., Bjørk, A., Gåseidnes, S., Sirevåg, R., Synstad, B., van den Burg, B., and Vriend, G. (2004) Rational engineering of enzyme stability. *J. Biotechnol.* **113,** 105–120
25. Tsou, C. L. (1993) Conformational flexibility of enzyme active sites. *Science* **262,** 380–381
26. Tsou, C. L. (1995) Inactivation precedes overall molecular conformation changes during enzyme denaturation. *Biochim. Biophys. Acta* **1253,** 151–162
27. Jaeger, K. E., and Reetz, M. T. (1998) Microbial lipases form versatile tools for biotechnology. *Trends Biotechnol.* **16,** 396–403
28. Jaeger, K. E., and Eggert, T. (2002) Lipases for biotechnology. *Curr. Opin. Biotechnol.* **13,** 390–397
29. Hasan, F., Shah, A. A., and Hameed, A. (2006) Industrial applications of microbial lipases. *Enzyme Microb. Technol.* **39,** 235–251
30. Treichel, H., Oliveira, D., Mazutti, M. A., Luccio, M., and Oliveira, J. V. (2010) A review on microbial lipases production. *Food Bioprocess Technol.* **3,** 182–196
31. Singh, A. K., and Mukhopadhyay, M. (2012) Overview of fungal lipase: a review. *Appl. Biochem. Biotechnol.* **166,** 486–520
32. Zhang, N., Suen, W. C., Windsor, W., Xiao, L., Madison, V., and Zaks, A. (2003) Improving tolerance of *Candida antarctica* lipase B towards irreversible thermal inactivation through directed evolution. *Protein Eng.* **16,** 599–605
33. Larsen, M. W., Bornscheuer, U. T., and Hult, K. (2008) Expression of *Candida antarctica* lipase B in *Pichia pastoris* and various *Escherichia coli* systems. *Protein Expr. Purif.* **62,** 90–97
34. Kim, S. J., Lee, J. A., Joo, J. C., Yoo, Y. J., Kim, Y. H., and Song, B. K. (2010) The development of a thermostable CiP (*Coprinus cinereus* peroxidase) through *in silico* design. *Biotechnol. Prog.* **26,** 1038–1046
35. Wulf, H., Mallin, H., and Bornscheuer, U. T. (2012) Protein engineering of a thermostable polyol dehydrogenase. *Enzyme Microb. Technol.* **51,** 217–224
36. Li, B., Yang, G., Wu, L., and Feng, Y. (2012) Role of the NC-loop in catalytic activity and stability in lipase from *Fervidobacterium changbaicum*. *PLoS One* **7,** e46881
37. Tina, K. G., Bhadra, R., and Srinivasan, N. (2007) PIC: Protein Interactions Calculator. *Nucleic Acids Res.* **35,** W473–W476
38. Van Der Spoel, D., Lindahl, E., Hess, B., Groenhof, G., Mark, A. E., and Berendsen, H. J. (2005) GROMACS: fast, flexible, and free. *J. Comput. Chem.* **26,** 1701–1718
39. Uppenberg, J., Hansen, M. T., Patkar, S., and Jones, T. A. (1994) The sequence, crystal structure determination and refinement of two crystal forms of lipase B from *Candida antarctica*. *Structure* **2,** 293–308
40. Reetz, M. T., and Carballeira, J. D. (2007) Iterative saturation mutagenesis (ISM) for rapid directed evolution of functional enzymes. *Nat. Protoc.* **2,** 891–903
41. Reetz, M. T., Kahakeaw, D., and Lohmer, R. (2008) Addressing the numbers problem in directed evolution. *ChemBioChem* **9,** 1797–1804
42. Skjøt, M., De Maria, L., Chatterjee, R., Svendsen, A., Patkar, S. A., Ostergaard, P. R., and Brask, J. (2009) Understanding the plasticity of the α/β hydrolase fold: lid swapping on the *Candida antarctica* lipase B results in chimeras with interesting biocatalytic properties. *ChemBioChem* **10,** 520–527
43. Koudelakova, T., Chaloupkova, R., Brezovsky, J., Prokop, Z., Sebestova, E., Hesseler, M., Khabiri, M., Plevaka, M., Kulik, D., Kuta Smatanova, I., Rezacova, P., Ettrich, R., Bornscheuer, U. T., and Damborsky, J. (2013) Engineering enzyme stability and resistance to an organic cosolvent by modification of residues in the access tunnel. *Angew. Chem. Int. Ed. Engl.* **52,** 1959–1963
44. Ahmad, S., Kamal, M. Z., Sankaranarayanan, R., and Rao, N. M. (2008) Thermostable *Bacillus subtilis* lipases: *in vitro* evolution and structural insight. *J. Mol. Biol.* **381,** 324–340

Downloaded from http://www.jbc.org/ at BIRMINGHAM SOUTHERN COLLEGE on October 9, 2017

Enhanced Enzyme Kinetic Stability by Increasing Rigidity within the Active Site

Yuan Xie, Jiao An, Guangyu Yang, Geng Wu, Yong Zhang, Li Cui and Yan Feng

J. Biol. Chem. 2014, 289:7994-8006.
doi: 10.1074/jbc.M113.536045 originally published online January 21, 2014

Access the most updated version of this article at doi: 10.1074/jbc.M113.536045

Alerts:
- When this article is cited
- When a correction for this article is posted

Click here to choose from all of JBC's e-mail alerts

Supplemental material:
http://www.jbc.org/content/suppl/2014/01/21/M113.536045.DC1

This article cites 44 references, 3 of which can be accessed free at
http://www.jbc.org/content/289/11/7994.full.html#ref-list-1

Downloaded from http://www.jbc.org/ at BIRMINGHAM SOUTHERN COLLEGE on October 9, 2017